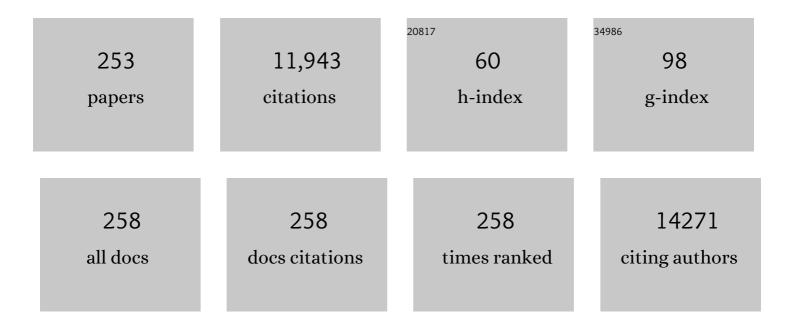
## Stefan Vogt

List of Publications by Year in descending order

Source: https://exaly.com/author-pdf/6240308/publications.pdf Version: 2024-02-01



STEEAN VOCT

#	Article	IF	CITATIONS
1	Uptake and Distribution of Ultrasmall Anatase TiO <sub>2</sub> Alizarin Red S Nanoconjugates in <i>Arabidopsis thaliana</i> . Nano Letters, 2010, 10, 2296-2302.	9.1	395
2	Imaging of the intracellular topography of copper with a fluorescent sensor and by synchrotron x-ray fluorescence microscopy. Proceedings of the National Academy of Sciences of the United States of America, 2005, 102, 11179-11184.	7.1	351
3	Biology of TiO2–oligonucleotide nanocomposites. Nature Materials, 2003, 2, 343-346.	27.5	286
4	Mechanisms of gold biomineralization in the bacterium <i>Cupriavidus metallidurans</i> . Proceedings of the United States of America, 2009, 106, 17757-17762.	7.1	283
5	Nanometer Linear Focusing of Hard X Rays by a Multilayer Laue Lens. Physical Review Letters, 2006, 96, 127401.	7.8	257
6	COPPER AND ANGIOGENESIS: UNRAVELLING A RELATIONSHIP KEY TO CANCER PROGRESSION. Clinical and Experimental Pharmacology and Physiology, 2009, 36, 88-94.	1.9	251
7	Quantifying Trace Elements in Individual Aquatic Protist Cells with a Synchrotron X-ray Fluorescence Microprobe. Analytical Chemistry, 2003, 75, 3806-3816.	6.5	216
8	X-ray fluorescence microprobe imaging in biology and medicine. Journal of Cellular Biochemistry, 2006, 99, 1489-1502.	2.6	213
9	Zinc availability regulates exit from meiosis in maturing mammalian oocytes. Nature Chemical Biology, 2010, 6, 674-681.	8.0	208
10	Focusing of hard x-rays to 16 nanometers with a multilayer Laue lens. Applied Physics Letters, 2008, 92, 221114.	3.3	190
11	Quantitative mapping of zinc fluxes in the mammalian egg reveals the origin of fertilization-induced zinc sparks. Nature Chemistry, 2015, 7, 130-139.	13.6	185
12	Zinc Sparks Are Triggered by Fertilization and Facilitate Cell Cycle Resumption in Mammalian Eggs. ACS Chemical Biology, 2011, 6, 716-723.	3.4	184
13	Calcium-dependent copper redistributions in neuronal cells revealed by a fluorescent copper sensor and X-ray fluorescence microscopy. Proceedings of the National Academy of Sciences of the United States of America, 2011, 108, 5980-5985.	7.1	182
14	Cluster analysis of soft X-ray spectromicroscopy data. Ultramicroscopy, 2004, 100, 35-57.	1.9	180
15	X-ray fluorescence microscopy reveals large-scale relocalization and extracellular translocation of cellular copper during angiogenesis. Proceedings of the National Academy of Sciences of the United States of America, 2007, 104, 2247-2252.	7.1	178
16	Synthesis, Characterization, and <i>in Vitro</i> Testing of Superparamagnetic Iron Oxide Nanoparticles Targeted Using Folic Acid-Conjugated Dendrimers. ACS Nano, 2008, 2, 773-783.	14.6	163
17	Nanoparticles for Applications in Cellular Imaging. Nanoscale Research Letters, 2007, 2, 430-41.	5.7	158
18	Zinc Concentration in Esophageal Biopsy Specimens Measured by X-Ray Fluorescence and Esophageal Cancer Risk. Journal of the National Cancer Institute, 2005, 97, 301-306.	6.3	153

#	Article	IF	CITATIONS
19	Hard X-ray fluorescence tomography—an emerging tool for structural visualization. Current Opinion in Structural Biology, 2010, 20, 606-614.	5.7	153
20	The Bionanoprobe: hard X-ray fluorescence nanoprobe with cryogenic capabilities. Journal of Synchrotron Radiation, 2014, 21, 66-75.	2.4	151
21	MAPS : A set of software tools for analysis and visualization of 3D X-ray fluorescence data sets. European Physical Journal Special Topics, 2003, 104, 635-638.	0.2	147
22	Quantitative 3D elemental microtomography of <i>Cyclotella meneghiniana</i> at 400-nm resolution. Proceedings of the National Academy of Sciences of the United States of America, 2010, 107, 15676-15680.	7.1	146
23	Simultaneous cryo X-ray ptychographic and fluorescence microscopy of green algae. Proceedings of the United States of America, 2015, 112, 2314-2319.	7.1	146
24	Nuclear microprobe – synchrotron synergy: Towards integrated quantitative real-time elemental imaging using PIXE and SXRF. Nuclear Instruments & Methods in Physics Research B, 2005, 231, 183-188.	1.4	129
25	Takagi-Taupin description of x-ray dynamical diffraction from diffractive optics with large numerical aperture. Physical Review B, 2007, 76, .	3.2	128
26	Radiation damage in protein crystals is reduced with a micron-sized X-ray beam. Proceedings of the National Academy of Sciences of the United States of America, 2011, 108, 6127-6132.	7.1	124
27	Increased brain iron coincides with early plaque formation in a mouse model of Alzheimer's disease. NeuroImage, 2011, 55, 32-38.	4.2	123
28	Intracellular Distribution of TiO2â^'DNA Oligonucleotide Nanoconjugates Directed to Nucleolus and Mitochondria Indicates Sequence Specificity. Nano Letters, 2007, 7, 596-601.	9.1	116
29	Levels of Zinc, Selenium, Calcium, and Iron in Benign Breast Tissue and Risk of Subsequent Breast Cancer. Cancer Epidemiology Biomarkers and Prevention, 2007, 16, 1682-1685.	2.5	113
30	Epidermal Growth Factor Receptor Targeted Nuclear Delivery and High-Resolution Whole Cell X-ray Imaging of Fe <sub>3</sub> O <sub>4</sub> @TiO <sub>2</sub> Nanoparticles in Cancer Cells. ACS Nano, 2013, 7, 10502-10517.	14.6	113
31	DNAâ^'TiO2 Nanoconjugates Labeled with Magnetic Resonance Contrast Agents. Journal of the American Chemical Society, 2007, 129, 15760-15761.	13.7	105
32	Zernike phase contrast in scanning microscopy with X-rays. Nature Physics, 2010, 6, 883-887.	16.7	105
33	Metal quotas of plankton in the equatorial Pacific Ocean. Deep-Sea Research Part II: Topical Studies in Oceanography, 2011, 58, 325-341.	1.4	103
34	Continuous motion scan ptychography: characterization for increased speed in coherent x-ray imaging. Optics Express, 2015, 23, 5438.	3.4	102
35	Nanocarriers Enhance Doxorubicin Uptake in Drug-Resistant Ovarian Cancer Cells. Cancer Research, 2012, 72, 769-778.	0.9	97
36	Significant silicon accumulation by marine picocyanobacteria. Nature Geoscience, 2012, 5, 886-891.	12.9	96

#	Article	IF	CITATIONS
37	Labeling TiO <sub>2</sub> Nanoparticles with Dyes for Optical Fluorescence Microscopy and Determination of TiO <sub>2</sub> –DNA Nanoconjugate Stability. Small, 2009, 5, 1318-1325.	10.0	95
38	Wilson Disease at a Single Cell Level. Journal of Biological Chemistry, 2010, 285, 30875-30883.	3.4	95
39	Quantitative Phase Imaging with a Scanning Transmission X-Ray Microscope. Physical Review Letters, 2008, 100, 163902.	7.8	93
40	X-ray ptychographic and fluorescence microscopy of frozen-hydrated cells using continuous scanning. Scientific Reports, 2017, 7, 445.	3.3	88
41	Scientific data exchange: a schema for HDF5-based storage of raw and analyzed data. Journal of Synchrotron Radiation, 2014, 21, 1224-1230.	2.4	86
42	Correlative microXRF and optical immunofluorescence microscopy of adherent cells labeled with ultrasmall gold particles. Journal of Structural Biology, 2006, 155, 22-29.	2.8	84
43	Differential remineralization of major and trace elements in sinking diatoms. Limnology and Oceanography, 2014, 59, 689-704.	3.1	84
44	Preserving elemental content in adherent mammalian cells for analysis by synchrotronâ€based xâ€ray fluorescence microscopy. Journal of Microscopy, 2017, 265, 81-93.	1.8	83
45	Metal contents of phytoplankton and labile particulate material in the North Atlantic Ocean. Progress in Oceanography, 2015, 137, 261-283.	3.2	81
46	Correlative 3D x-ray fluorescence and ptychographic tomography of frozen-hydrated green algae. Science Advances, 2018, 4, eaau4548.	10.3	79
47	Ductal Carcinoma in Situ: X-ray Fluorescence Microscopy and Dynamic Contrast-enhanced MR Imaging Reveals Gadolinium Uptake within Neoplastic Mammary Ducts in a Murine Model. Radiology, 2009, 253, 399-406.	7.3	76
48	An iron-dependent and transferrin-mediated cellular uptake pathway for plutonium. Nature Chemical Biology, 2011, 7, 560-565.	8.0	76
49	Differential phase contrast with a segmented detector in a scanning X-ray microprobe. Journal of Synchrotron Radiation, 2008, 15, 355-362.	2.4	75
50	Simultaneous X-ray fluorescence and ptychographic microscopy of Cyclotella meneghiniana. Optics Express, 2012, 20, 18287.	3.4	75
51	Cluster analysis in soft X-ray spectromicroscopy: Finding the patterns in complex specimens. Journal of Electron Spectroscopy and Related Phenomena, 2005, 144-147, 1137-1143.	1.7	74
52	Unexpected Role of the Copper Transporter ATP7A in PDGF-Induced Vascular Smooth Muscle Cell Migration. Circulation Research, 2010, 107, 787-799.	4.5	73
53	Metabolism of Selenite in Human Lung Cancer Cells: X-Ray Absorption and Fluorescence Studies. Journal of the American Chemical Society, 2011, 133, 18272-18279.	13.7	73
54	Silicon nitride as a versatile growth substrate for microspectroscopic imaging and mapping of individual cells. Molecular BioSystems, 2010, 6, 1316.	2.9	72

#	Article	IF	CITATIONS
55	Zinc sparks induce physiochemical changes in the egg zona pellucida that prevent polyspermy. Integrative Biology (United Kingdom), 2017, 9, 135-144.	1.3	72
56	X-Ray Spectromicroscopy—A Tool for Environmental Sciences. Environmental Science & Technology, 2007, 41, 6885-6889.	10.0	70
57	Synchrotron-based X-ray Fluorescence Microscopy in Conjunction with Nanoindentation to Study Molecular-Scale Interactions of Phenol–Formaldehyde in Wood Cell Walls. ACS Applied Materials & Interfaces, 2015, 7, 6584-6589.	8.0	70
58	X-Ray Fluorescence Microscopy Reveals the Role of Selenium in Spermatogenesis. Journal of Molecular Biology, 2009, 389, 808-818.	4.2	65
59	Multiple protective activities of neuroglobin in cultured neuronal cells exposed to hypoxia reâ€oxygenation injury. Journal of Neurochemistry, 2009, 108, 1143-1154.	3.9	63
60	Role of biogenic silica in the removal of iron from the Antarctic seas. Nature Communications, 2013, 4, 1981.	12.8	61
61	The Velociprobe: An ultrafast hard X-ray nanoprobe for high-resolution ptychographic imaging. Review of Scientific Instruments, 2019, 90, 083701.	1.3	61
62	Selenium Metabolism in Cancer Cells: The Combined Application of XAS and XFM Techniques to the Problem of Selenium Speciation in Biological Systems. Nutrients, 2013, 5, 1734-1756.	4.1	60
63	Multilayer Laue lenses as high-resolution x-ray optics. , 2004, 5539, 185.		58
64	Role of diatoms in nickel biogeochemistry in the ocean. Global Biogeochemical Cycles, 2012, 26, .	4.9	58
65	COMPUTED TOMOGRAPHY OF CRYOGENIC CELLS. Surface Review and Letters, 2002, 09, 177-183.	1.1	57
66	Role of Copper Transport Protein Antioxidant 1 in Angiotensin II–Induced Hypertension. Hypertension, 2012, 60, 476-486.	2.7	57
67	The Unique Biogeochemical Signature of the Marine Diazotroph Trichodesmium. Frontiers in Microbiology, 2012, 3, 150.	3.5	57
68	Endothelial Antioxidant-1: a Key Mediator of Copper-dependent Wound Healing in vivo. Scientific Reports, 2016, 6, 33783.	3.3	55
69	Carcinogenic Chromium(VI) Compounds Formed by Intracellular Oxidation of Chromium(III) Dietary Supplements by Adipocytes. Angewandte Chemie - International Edition, 2016, 55, 1742-1745.	13.8	54
70	Selectivity in biomineralization of barium and strontium. Journal of Structural Biology, 2011, 176, 192-202.	2.8	53
71	Quantitative comparison of preparation methodologies for x-ray fluorescence microscopy of brain tissue. Analytical and Bioanalytical Chemistry, 2011, 401, 853-864.	3.7	53
72	X-Ray Fluorescence Microscopy Reveals Accumulation and Secretion of Discrete Intracellular Zinc Pools in the Lactating Mouse Mammary Gland. PLoS ONE, 2010, 5, e11078.	2.5	52

#	Article	IF	CITATIONS
73	Imaging Metals in Proteins by Combining Electrophoresis with Rapid X-ray Fluorescence Mapping. ACS Chemical Biology, 2010, 5, 577-587.	3.4	52
74	Iron distribution through the developmental stages of Medicago truncatula nodules. Metallomics, 2013, 5, 1247.	2.4	52
75	Metal-deficient aggregates and diminished copper found in cells expressing SOD1 mutations that cause ALS. Frontiers in Aging Neuroscience, 2014, 6, 110.	3.4	52
76	Cell-Permeable MR Contrast Agents with Increased Intracellular Retention. Bioconjugate Chemistry, 2008, 19, 2049-2059.	3.6	51
77	Uptake, Distribution, and Speciation of Selenoamino Acids by Human Cancer Cells: X-ray Absorption and Fluorescence Methods. Biochemistry, 2011, 50, 1641-1650.	2.5	50
78	Highâ€resolution Xâ€ray imaging of <i>Plasmodium falciparum</i> â€infected red blood cells. Cytometry Part A: the Journal of the International Society for Analytical Cytology, 2008, 73A, 949-957.	1.5	49
79	Microprobe XRF Mapping and XAS Investigations of the Intracellular Metabolism of Arsenic for Understanding Arsenic-Induced Toxicity. Chemical Research in Toxicology, 2008, 21, 1760-1769.	3.3	49
80	Changes of the phagosomal elemental concentrations by Mycobacterium tuberculosis Mramp. Microbiology (United Kingdom), 2005, 151, 323-332.	1.8	47
81	Gadolinium-conjugated TiO2-DNA oligonucleotide nanoconjugates show prolonged intracellular retention period and T1-weighted contrast enhancement in magnetic resonance images. Nanomedicine: Nanotechnology, Biology, and Medicine, 2008, 4, 201-207.	3.3	46
82	3D imaging of transition metals in the zebrafish embryo by X-ray fluorescence microtomography. Metallomics, 2014, 6, 1648.	2.4	45
83	X-Ray Microscopic Studies of the Drosophila Dosage Compensation Complex. Journal of Structural Biology, 2000, 132, 123-132.	2.8	44
84	Selective Aggregation of a Platinum–Gadolinium Complex Within a Tumor ell Nucleus. Angewandte Chemie - International Edition, 2010, 49, 1231-1233.	13.8	44
85	High-Resolution Imaging of Selenium in Kidneys: A Localized Selenium Pool Associated with Glutathione Peroxidase 3. Antioxidants and Redox Signaling, 2012, 16, 185-192.	5.4	44
86	Copper Uptake, Intracellular Localization, and Speciation in Marine Microalgae Measured by Synchrotron Radiation X-ray Fluorescence and Absorption Microspectroscopy. Environmental Science & Technology, 2016, 50, 8827-8839.	10.0	44
87	Methylmercury Targets Photoreceptor Outer Segments. ACS Chemical Biology, 2013, 8, 2256-2263.	3.4	40
88	Imaging trace element distributions in single organelles and subcellular features. Scientific Reports, 2016, 6, 21437.	3.3	39
89	Synchrotron-based X-ray fluorescence microscopy enables multiscale spatial visualization of ions involved in fungal lignocellulose deconstruction. Scientific Reports, 2017, 7, 41798.	3.3	38
90	Migration of mercury from dental amalgam through human teeth. Journal of Synchrotron Radiation, 2008, 15, 123-128.	2.4	37

#	Article	IF	CITATIONS
91	Elemental composition of equatorial Pacific diatoms exposed to additions of silicic acid and iron. Deep-Sea Research Part II: Topical Studies in Oceanography, 2011, 58, 512-523.	1.4	37
92	Selective Sequestration of Strontium in Desmid Green Algae by Biogenic Coâ€precipitation with Barite. ChemSusChem, 2011, 4, 470-473.	6.8	37
93	LOCALIZATION OF IRON WITHIN CENTRIC DIATOMS OF THE GENUS <i>THALASSIOSIRA</i> <sup>1</sup> . Journal of Phycology, 2012, 48, 626-634.	2.3	37
94	Non-negative matrix analysis for effective feature extraction in X-ray spectromicroscopy. Faraday Discussions, 2014, 171, 357-371.	3.2	37
95	Threshold for ion movements in wood cell walls below fiber saturation observed by X-ray fluorescence microscopy (XFM). Holzforschung, 2015, 69, 441-448.	1.9	36
96	A link between copper and dental caries in human teeth identified by X-ray fluorescence elemental mapping. Journal of Biological Inorganic Chemistry, 2008, 13, 303-306.	2.6	35
97	Variations in <i>Synechococcus</i> cell quotas of phosphorus, sulfur, manganese, iron, nickel, and zinc within mesoscale eddies in the Sargasso Sea. Limnology and Oceanography, 2010, 55, 492-506.	3.1	35
98	Reduced Utilization of Selenium by Naked Mole Rats Due to a Specific Defect in GPx1 Expression. Journal of Biological Chemistry, 2011, 286, 17005-17014.	3.4	35
99	Opportunities in multidimensional trace metal imaging: taking copper-associated disease research to the next level. Analytical and Bioanalytical Chemistry, 2013, 405, 1809-1820.	3.7	35
100	Fresnel zone plate stacking in the intermediate field for high efficiency focusing in the hard X-ray regime. Optics Express, 2014, 22, 28142.	3.4	35
101	The †̃Tully monster' is a vertebrate. Nature, 2016, 532, 496-499.	27.8	35
102	Regulatory properties and cellular redistribution of zinc during macrophage differentiation of human leukemia cells. Journal of Structural Biology, 2006, 155, 2-11.	2.8	34
103	Exploring Ocean Biogeochemistry by Singleâ€Cell Microprobe Analysis of Protist Elemental Composition <sup>1</sup> . Journal of Eukaryotic Microbiology, 2008, 55, 151-162.	1.7	34
104	Biomedical applications of X-ray absorption and vibrational spectroscopic microscopies in obtaining structural information from complex systems. Radiation Physics and Chemistry, 2010, 79, 176-184.	2.8	34
105	Bovine eggs release zinc in response to parthenogenetic and sperm-induced egg activation. Theriogenology, 2019, 127, 41-48.	2.1	34
106	Quantification of phosphorus in single cells using synchrotron X-ray fluorescence. Journal of Synchrotron Radiation, 2010, 17, 560-566.	2.4	33
107	Encapsulation, controlled release, and antitumor efficacy of cisplatin delivered in liposomes composed of sterol-modified phospholipids. European Journal of Pharmaceutical Sciences, 2017, 103, 85-93.	4.0	33
108	Intracellular distributions of essential elements in cardiomyocytes. Journal of Structural Biology, 2006, 155, 12-21.	2.8	32

#	Article	IF	CITATIONS
109	Quantitative Imaging of Cell-Permeable Magnetic Resonance Contrast Agents Using X-Ray Fluorescence. Molecular Imaging, 2006, 5, 7290.2006.00026.	1.4	32
110	Cementum structure in Beluga whale teeth. Acta Biomaterialia, 2017, 48, 289-299.	8.3	32
111	Periplasmic response upon disruption of transmembrane Cu transport in Pseudomonas aeruginosa. Metallomics, 2013, 5, 144.	2.4	31
112	Intracellular distribution and stability of a luminescent rhenium( <scp>i</scp> ) tricarbonyl tetrazolato complex using epifluorescence microscopy in conjunction with X-ray fluorescence imaging. Metallomics, 2017, 9, 382-390.	2.4	31
113	XAS and XFM studies of selenium and copper speciation and distribution in the kidneys of selenite-supplemented rats. Metallomics, 2014, 6, 1602-1615.	2.4	30
114	Multiscale deconstruction of molecular architecture in corn stover. Scientific Reports, 2014, 4, 3756.	3.3	30
115	Intracellular in situ labeling of TiO2 nanoparticles for fluorescence microscopy detection. Nano Research, 2018, 11, 464-476.	10.4	30
116	Variations in Synechococcus cell quotas of phosphorus, sulfur, manganese, iron, nickel, and zinc within mesoscale eddies in the Sargasso Sea. Limnology and Oceanography, 2010, 55, 492-506.	3.1	30
117	Virulence-related Mycobacterium avium subsp hominissuis MAV_2928 gene is associated with vacuole remodeling in macrophages. BMC Microbiology, 2010, 10, 100.	3.3	29
118	Optimizing detector geometry for trace element mapping by X-ray fluorescence. Ultramicroscopy, 2015, 152, 44-56.	1.9	29
119	Acetylation increases relative humidity threshold for ion transport in wood cell walls – A means to understanding decay resistance. International Biodeterioration and Biodegradation, 2018, 133, 230-237.	3.9	29
120	Distribution and speciation of gold in biogenic and abiogenic calcium carbonates – Implications for the formation of gold anomalous calcrete. Geochimica Et Cosmochimica Acta, 2011, 75, 1942-1956.	3.9	28
121	X-ray methods to observe and quantify adhesive penetration into wood. Journal of Materials Science, 2019, 54, 705-718.	3.7	28
122	Copper Transporter ATP7A (Copper-Transporting P-Type ATPase/Menkes ATPase) Limits Vascular Inflammation and Aortic Aneurysm Development. Arteriosclerosis, Thrombosis, and Vascular Biology, 2019, 39, 2320-2337.	2.4	28
123	Evidence for strain compensation in stabilizing epitaxial growth of highly doped germanium. Physical Review B, 2004, 69, .	3.2	27
124	Elemental analysis of the Mycobacterium avium phagosome in Balb/c mouse macrophages. Biochemical and Biophysical Research Communications, 2006, 344, 1346-1351.	2.1	27
125	Intracellular Targeting and Pharmacological Activity of the Superoxide Dismutase Mimics MnTE-2-PyP <sup>5+</sup> and MnTnHex-2-PyP <sup>5+</sup> Regulated by Their Porphyrin Ring Substituents. Inorganic Chemistry, 2013, 52, 4121-4123.	4.0	27
126	X-ray fluorescence at nanoscale resolution for multicomponent layered structures: a solar cell caseÂstudy. Journal of Synchrotron Radiation, 2017, 24, 288-295.	2.4	27

#	Article	IF	CITATIONS
127	Data analysis for X-ray fluorescence imaging. European Physical Journal Special Topics, 2003, 104, 617-622.	0.2	26
128	X-Ray Fluorescence Microscopy for Investigation of Archival Tissues. Health Physics, 2012, 103, 181-186.	0.5	25
129	The inorganic anatomy of the mammalian preimplantation embryo and the requirement of zinc during the first mitotic divisions. Developmental Dynamics, 2015, 244, 935-947.	1.8	25
130	Mechanisms of murine cerebral malaria: Multimodal imaging of altered cerebral metabolism and protein oxidation at hemorrhage sites. Science Advances, 2015, 1, e1500911.	10.3	25
131	The 2-ID-B intermediate-energy scanning X-ray microscope at the APS. European Physical Journal Special Topics, 2003, 104, 11-15.	0.2	24
132	Ultraviolet Germicidal Irradiation and Its Effects on Elemental Distributions in Mouse Embryonic Fibroblast Cells in X-Ray Fluorescence Microanalysis. PLoS ONE, 2015, 10, e0117437.	2.5	24
133	Alignment of low-dose X-ray fluorescence tomographyÂimages using differential phase contrast. Journal of Synchrotron Radiation, 2014, 21, 229-234.	2.4	24
134	Dark field X-ray microscopy: the effects of condenser/detector aperture. Ultramicroscopy, 2001, 87, 25-44.	1.9	23
135	Composition characterization of combinatorial materials by scanning X-ray fluorescence microscopy using microfocused synchrotron X-ray beam. Applied Surface Science, 2004, 223, 214-219.	6.1	23
136	Mechanism of Selenium-Induced Inhibition of Arsenic-Enhanced UVR Carcinogenesis in Mice. Environmental Health Perspectives, 2008, 116, 703-708.	6.0	23
137	Characterization of phosphorus, calcium, iron, and other elements in organisms at subâ€micron resolution using Xâ€ray fluorescence spectromicroscopy. Limnology and Oceanography: Methods, 2009, 7, 42-51.	2.0	23
138	PAST AND FUTURE WORK ON RADIOBIOLOGY MEGA-STUDIES: A CASE STUDY AT ARGONNE NATIONAL LABORATORY. Health Physics, 2011, 100, 613-621.	0.5	23
139	Identifying metalloproteins through X-ray fluorescence mapping and mass spectrometry. Metallomics, 2012, 4, 921.	2.4	22
140	Tomographic imaging of biological specimens with the cryo transmission X-ray microscope. Nuclear Instruments and Methods in Physics Research, Section A: Accelerators, Spectrometers, Detectors and Associated Equipment, 2001, 467-468, 1308-1311.	1.6	21
141	X-ray fluorescence imaging of single human cancer cells reveals that the N-heterocyclic ligands of iodinated analogues of ruthenium anticancer drugs remain coordinated after cellular uptake. Journal of Biological Inorganic Chemistry, 2013, 18, 845-853.	2.6	21
142	Quantitation and localization of intracellular redox active metals by X-ray fluorescence microscopy in cortical neurons derived from APP and APLP2 knockout tissue. Metallomics, 2014, 6, 1894-1904.	2.4	21
143	Intracellular concentration map of magnesium in whole cells by combined use of X-ray fluorescence microscopy and atomic force microscopy. Spectrochimica Acta, Part B: Atomic Spectroscopy, 2011, 66, 834-840.	2.9	20
144	Broadband X-ray ptychography using multi-wavelength algorithm. Journal of Synchrotron Radiation, 2021, 28, 309-317.	2.4	20

#	Article	IF	CITATIONS
145	Cell wall targeted <i>in planta</i> iron accumulation enhances biomass conversion and seed iron concentration in Arabidopsis and rice. Plant Biotechnology Journal, 2016, 14, 1998-2009.	8.3	19
146	Plutonium uptake and distribution in mammalian cells: Molecular vs. polymeric plutonium. International Journal of Radiation Biology, 2011, 87, 1023-1032.	1.8	18
147	Measurement of moisture-dependent ion diffusion constants in wood cell wall layers using time-lapse micro X-ray fluorescence microscopy. Scientific Reports, 2020, 10, 9919.	3.3	18
148	Loss of Pluripotency in Human Embryonic Stem Cells Directly Correlates with an Increase in Nuclear Zinc. PLoS ONE, 2010, 5, e12308.	2.5	18
149	Structural investigation of CoMnGe combinatorial epitaxial thin films using microfocused synchrotron X-ray. Applied Surface Science, 2004, 223, 175-182.	6.1	17
150	Self-Assembled, Mesoporous Polymeric Networks for Patterned Protein Arrays. Langmuir, 2005, 21, 10301-10306.	3.5	17
151	THE OXIDATION STATE OF EUROPIUM IN HYDROTHERMAL SCHEELITE: IN SITU MEASUREMENT BY XANES SPECTROSCOPY. Canadian Mineralogist, 2006, 44, 1079-1087.	1.0	17
152	Optomechanical Design of a Hard X-ray Nanoprobe Instrument with Nanometer-Scale Active Vibration Control. AIP Conference Proceedings, 2007, , .	0.4	17
153	Trends in X-ray Fluorescence Microscopy. Synchrotron Radiation News, 2013, 26, 32-38.	0.8	17
154	Quantitative imaging of cell-permeable magnetic resonance contrast agents using x-ray fluorescence. Molecular Imaging, 2006, 5, 485-97.	1.4	17
155	A shutter–photodiode combination for UV and soft X-ray beamlines. Journal of Synchrotron Radiation, 1999, 6, 50-50.	2.4	16
156	<i>β</i> â€Cell subcellular localization of glucoseâ€stimulated Mn uptake by Xâ€ray fluorescence microscopy: implications for pancreatic MRI. Contrast Media and Molecular Imaging, 2011, 6, 474-481.	0.8	16
157	Synchrotron radiation induced X-ray emission studies of the antioxidant mechanism of the organoselenium drug ebselen. Journal of Biological Inorganic Chemistry, 2012, 17, 589-598.	2.6	16
158	Tissue specific specialization of the nanoscale architecture of Arabidopsis. Journal of Structural Biology, 2013, 184, 103-114.	2.8	16
159	(Pentamethylcyclopentadienato)rhodium Complexes for Delivery of the Curcumin Anticancer Drug. European Journal of Inorganic Chemistry, 2017, 2017, 1812-1823.	2.0	16
160	Quantifying X-Ray Fluorescence Data Using MAPS. Journal of Visualized Experiments, 2018, , .	0.3	16
161	Direct Determination of the Intracellular Oxidation State of Plutonium. Inorganic Chemistry, 2011, 50, 7591-7597.	4.0	15
162	Achieving high spatial resolution in a large field-of-view using lensless x-ray imaging. Applied Physics Letters, 2021, 119, .	3.3	15

#	Article	IF	CITATIONS
163	Rapid and Accurate Analysis of an X-Ray Fluorescence Microscopy Data Set through Gaussian Mixture-Based Soft Clustering Methods. Microscopy and Microanalysis, 2013, 19, 1281-1289.	0.4	14
164	A Next-Generation Hard X-Ray Nanoprobe Beamline for In Situ Studies of Energy Materials and Devices. Metallurgical and Materials Transactions A: Physical Metallurgy and Materials Science, 2014, 45, 85-97.	2.2	14
165	MicroXRF tomographic visualization of zinc and iron in the zebrafish embryo at the onset of the hatching period. Metallomics, 2016, 8, 1122-1130.	2.4	14
166	Combinatorial synthesis and characterization of a ternary epitaxial film of Co and Mn doped Ge (001). Applied Surface Science, 2007, 254, 709-713.	6.1	13
167	The Bionanoprobe: Synchrotron-Based Hard X-ray Fluorescence Microscopy for 2D/3D Trace Element Mapping. Microscopy Today, 2015, 23, 26-29.	0.3	13
168	Microplankton trace element contents: implications for mineral limitation of mesozooplankton in an HNLC area. Journal of Plankton Research, 2016, 38, 256-270.	1.8	13
169	Trace Metal Imaging of Sulfate-Reducing Bacteria and Methanogenic Archaea at Single-Cell Resolution by Synchrotron X-Ray Fluorescence Imaging. Geomicrobiology Journal, 2018, 35, 81-89.	2.0	13
170	Performance and Ongoing Development of the Velociprobe, a Fast Hard X-ray Nanoprobe for High-Resolution Ptychographic Imaging. Microscopy and Microanalysis, 2018, 24, 54-55.	0.4	13
171	The application of synchrotron radiation induced X-ray emission in the measurement of zinc and lead in Wistar rat ameloblasts. Archives of Oral Biology, 2007, 52, 938-944.	1.8	12
172	Biological applications of X-ray microprobes. International Journal of Radiation Biology, 2009, 85, 710-713.	1.8	12
173	Directed plant cell-wall accumulation of iron: embedding co-catalyst for efficient biomass conversion. Biotechnology for Biofuels, 2016, 9, 225.	6.2	12
174	Imaging of Vanadium in Microfossils: A New Potential Biosignature. Astrobiology, 2017, 17, 1069-1076.	3.0	12
175	A robot-based detector manipulator system for a hard X-ray nanoprobe instrument. Nuclear Instruments and Methods in Physics Research, Section A: Accelerators, Spectrometers, Detectors and Associated Equipment, 2007, 582, 159-161.	1.6	10
176	Uptake and Distribution of a Platinum(II)-Carborane Complex Within a Tumour Cell Using Synchrotron XRF Imaging. Australian Journal of Chemistry, 2011, 64, 253.	0.9	10
177	Elemental Profiling of Single Bacterial Cells As a Function of Copper Exposure and Growth Phase. PLoS ONE, 2011, 6, e21255.	2.5	10
178	Synchrotron X-ray fluorescence studies of a bromine-labelled cyclic RGD peptide interacting with individual tumor cells. Journal of Synchrotron Radiation, 2013, 20, 226-233.	2.4	10
179	X-Ray Fluorescence Microscopy Demonstrates Preferential Accumulation of a Vanadium-Based Magnetic Resonance Imaging Contrast Agent in Murine Colonic Tumors. Molecular Imaging, 2015, 14, 7290.2015.00001.	1.4	10
180	Copper, zinc and calcium: imaging and quantification in anterior pituitary secretory granules. Metallomics, 2016, 8, 1012-1022.	2.4	10

#	Article	IF	CITATIONS
181	Increased Throughput and Sensitivity of Synchrotron-Based Characterization for Photovoltaic Materials. IEEE Journal of Photovoltaics, 2017, 7, 763-771.	2.5	10
182	Multi-beam X-ray ptychography for high-throughput coherent diffraction imaging. Scientific Reports, 2020, 10, 19550.	3.3	10
183	Cluster analysis of soft X-ray spectromicroscopy data. European Physical Journal Special Topics, 2003, 104, 623-626.	0.2	10
184	Unsupervised cell identification on multidimensional X-ray fluorescence datasets. Journal of Synchrotron Radiation, 2014, 21, 568-579.	2.4	10
185	One-Micron Beams for Macromolecular Crystallography at GMâ^•CA-CAT. , 2010, , .		9
186	Development of Fe3O4 core–TiO2 shell nanocomposites and nanoconjugates as a foundation for neuroblastoma radiosensitization. Cancer Nanotechnology, 2021, 12, 12.	3.7	9
187	Structure and magnetism of Coa(1â^'x)MnaxGeb epitaxial films. Applied Surface Science, 2006, 252, 2512-2517.	6.1	8
188	A method for phase reconstruction from measurements obtained using a configured detector with a scanning transmission X-ray microscope. Nuclear Instruments and Methods in Physics Research, Section A: Accelerators, Spectrometers, Detectors and Associated Equipment, 2007, 582, 218-220.	1.6	8
189	Optimization-based simultaneous alignment and reconstruction in multi-element tomography. Optics Letters, 2019, 44, 4331.	3.3	8
190	Conceptual Design For A Beamline For A Hard x-ray Nanoprobe with 30 nm Spatial Resolution. AIP Conference Proceedings, 2004, , .	0.4	7
191	Fast Differential Phase-Contrast Imaging and Total Fluorescence Yield Mapping in a Hard X-ray Fluorescence Microprobe. AIP Conference Proceedings, 2004, , .	0.4	7
192	Submicron hard X-ray fluorescence imaging of synthetic elements. Analytica Chimica Acta, 2012, 722, 21-28.	5.4	7
193	Distribution of Iron Oxide Core-Titanium Dioxide Shell Nanoparticles in VX2 Tumor Bearing Rabbits Introduced by Two Different Delivery Modalities. Nanomaterials, 2016, 6, 143.	4.1	7
194	Carcinogenic Chromium(VI) Compounds Formed by Intracellular Oxidation of Chromium(III) Dietary Supplements by Adipocytes. Angewandte Chemie, 2016, 128, 1774-1777.	2.0	7
195	Investigation into the intracellular fates, speciation and mode of action of selenium-containing neuroprotective agents using XAS and XFM. Biochimica Et Biophysica Acta - General Subjects, 2018, 1862, 2393-2404.	2.4	7
196	IV Administered Gadodiamide Enters the Lumen of the Prostatic Glands: X-Ray Fluorescence Microscopy Examination of a Mouse Model. American Journal of Roentgenology, 2015, 205, W313-W319.	2.2	6
197	Microdistribution of lead in human teeth using microbeam synchrotron radiation X-ray fluorescence (μ-SRXRF). X-Ray Spectrometry, 2017, 46, 19-26.	1.4	6
198	Fungal–copper interactions in wood examined with large field of view synchrotron-based X-ray fluorescence microscopy. Wood Material Science and Engineering, 2019, 14, 174-184.	2.3	6

#	Article	IF	CITATIONS
199	Copper distribution and oxidation states near corroded fasteners in treated wood. SN Applied Sciences, 2019, 1, 1.	2.9	6
200	High resolution X-ray tomography with applications in biology and materials science. European Physical Journal Special Topics, 2003, 104, 607-613.	0.2	5
201	A Multimodal Nanocomposite for Biomedical Imaging. AIP Conference Proceedings, 2011, 1365, 379.	0.4	5
202	Micro X-ray Fluorescence Study of Late Pre-Hispanic Ceramics from the Western Slopes of the South Central Andes Region in the <i>Arica y Parinacota</i> Region, Chile: A New Methodological Approach. Applied Spectroscopy, 2016, 70, 1759-1769.	2.2	5
203	2D/3D cryo x-ray fluorescence imaging at the bionanoprobe at the advanced photon source. AIP Conference Proceedings, 2016, , .	0.4	5
204	Dynamic zinc fluxes regulate meiotic progression in <i>Caenorhabditis elegans</i> . Biology of Reproduction, 2022, 107, 406-418.	2.7	5
205	Tapered tilted linear zone plates for focusing hard x-rays. , 2004, , .		4
206	Epitaxial growth of (FeCo)[sub x]Ge[sub 1â^'x](001). Journal of Vacuum Science & Technology B, 2007, 25, 1217.	1.3	4
207	Interrogation of EGFR-Targeted Uptake of TiO[sub 2] Nanoconjugates by X-ray Fluorescence Microscopy. , 2011, 1365, 423-426.		4
208	Three-dimensional Imaging of Crystalline Inclusions Embedded in Intact Maize Stalks. Scientific Reports, 2013, 3, 2843.	3.3	4
209	Mapping the subcellular localization of Fe <sub>3</sub> O <sub>4</sub> @TiO <sub>2</sub> nanoparticles by X-ray Fluorescence Microscopy. Journal of Physics: Conference Series, 2013, 463, 012020.	0.4	4
210	Development of Multi-Scale X-ray Fluorescence Tomography for Examination of Nanocomposite-Treated Biological Samples. Cancers, 2021, 13, 4497.	3.7	4
211	Intracellular localization of titanium dioxide-biomolecule nanocomposites. European Physical Journal Special Topics, 2003, 104, 317-319.	0.2	4
212	The evolution of hard x-ray tomography from the micrometer to the nanometer length scale. , 2004, , .		3
213	Selective x-ray Bragg spectrometry: optimizing fluorescence microprobe sensitivity for precious metals. X-Ray Spectrometry, 2007, 36, 111-121.	1.4	3
214	Quantitative scanning differential phase contrast microscopy. Journal of Physics: Conference Series, 2009, 186, 012006.	0.4	3
215	Optomechanical design of a modular K-B mirror mount system for x-ray microfocusing at the advanced photon source. , 2013, , .		3
216	Wood as inspiration for new stimuli-responsive structures and materials. , 2014, , .		3

Wood as inspiration for new stimuli-responsive structures and materials. , 2014, , . 216

#	Article	IF	CITATIONS
217	PlantPredict: Solar Performance Modeling Made Simple. , 2017, , .		3
218	Spatial distribution of metals within the liver acinus and their perturbation by PCB126. Environmental Science and Pollution Research, 2018, 25, 16427-16433.	5.3	3
219	Instrumentation and method developments of x-ray ptychography at the Advanced Photon Source. , 2019, , .		3
220	X-ray microscopic studies of labeled nuclear cell structures. AIP Conference Proceedings, 2000, , .	0.4	2
221	Mapping 3D X-ray Fluorescence Datasets to Elemental Distributions using Principal Component Analysis and Fitting. Microscopy and Microanalysis, 2005, 11, .	0.4	2
222	PIXE Real-Time Quantitative Image Projection Applied to Synchrotron XRF Imaging using the X-ray Fluorescence Microprobe. Microscopy and Microanalysis, 2005, 11, .	0.4	2
223	Hard X-ray Fluorescence Microscopy to Determine the Element Distribution of Soil Colloids in Aqueous Environment. , 2011, , .		2
224	Spatially Resolved Sulfur Speciation in Urban Soils. , 2011, , .		2
225	A next-generation in-situ nanoprobe beamline for the Advanced Photon Source. Proceedings of SPIE, 2013, , .	0.8	2
226	New Developments in Hard X-ray Fluorescence Microscopy for In-situ Investigations of Trace Element Distributions in Aqueous Systems of Soil Colloids. Journal of Physics: Conference Series, 2013, 463, 012005.	0.4	2
227	Simultaneous x-ray nano-ptychographic and fluorescence microscopy at the bionanoprobe. , 2015, , .		2
228	Opportunities and limitations for combined fly-scan ptychography and fluorescence microscopy. , 2015, 9592, .		2
229	Visualizing specific nuclear proteins in eukaryotic cells using soft X-ray microscopy. Nuclear Instruments and Methods in Physics Research, Section A: Accelerators, Spectrometers, Detectors and Associated Equipment, 2001, 467-468, 1312-1314.	1.6	1
230	Nanotomography of labeled cryogenic cells. , 2002, 4503, 156.		1
231	Design for an X-ray Nanoprobe Prototype with a Sub-10-nm Positioning Requirement. AIP Conference Proceedings, 2004, , .	0.4	1
232	Investigation of Fly Ash Particulates Using SEM, TEM and Synchrotron Microprobe Techniques. Microscopy and Microanalysis, 2005, 11, .	0.4	1
233	Beamline Design for a BioNanoprobe: Stability and Coherence. AIP Conference Proceedings, 2007, , .	0.4	1
234	Response to Guzzi & Pigatto'sComments onMigration of mercury from dental amalgam through human teethby H. H. Harriset al.(2008).J. Synchrotron Rad.15, 123–128. Journal of Synchrotron Radiation, 2009, 16, 437-438.	2.4	1

#	Article	IF	CITATIONS
235	Correlative X-ray Ptychographic and Fluorescence Imaging at the Advanced Photon Source. Microscopy and Microanalysis, 2019, 25, 1030-1031.	0.4	1
236	High-speed and Large Field-of-view Imaging via X-ray Fly-scan Ptychography. Microscopy and Microanalysis, 2019, 25, 46-47.	0.4	1
237	Use of X-Ray Fluorescence Microscopy for Studies on Research Models of Hepatocellular Carcinoma. Frontiers in Public Health, 2021, 9, 711506.	2.7	1
238	Ptychopy: GPU framework for ptychographic data analysis. , 2021, , .		1
239	210 Development of titanium dioxide-DNA nanocomposites for intracellular delivery and radiation-mediated dna scission. Radiotherapy and Oncology, 2006, 78, S73-S74.	0.6	Ο
240	Probing radiation damage with a 1-micron beam. Acta Crystallographica Section A: Foundations and Advances, 2008, 64, C179-C180.	0.3	0
241	Combined X-ray Microfluorescence and Atomic Force Microscopy Studies of Mg Distribution in Whole Cells. , 2011, , .		0
242	Radiation damage to protein crystals is reduced with a micron-sized X-ray beam. Acta Crystallographica Section A: Foundations and Advances, 2011, 67, C158-C158.	0.3	0
243	Sub-100-nm 3D-elemental mapping of frozen-hydrated cells using the bionanoprobe. Proceedings of SPIE, 2013, , .	0.8	0
244	Cryogenic Sample Preparation Preserves Elemental Composition for Correlative Light and X-ray Fluorescence Microscopy. Microscopy and Microanalysis, 2015, 21, 877-878.	0.4	0
245	Stacking multiple zone plates for efficient hard x-ray focusing at the Advanced Photon Source. Proceedings of SPIE, 2015, , .	0.8	0
246	HYBRID Simulations of Diffraction-Limited Focusing with Kirkpatrick-Baez Mirrors for a Next-Generation In Situ Hard X-ray Nanoprobe. Metallurgical and Materials Transactions A: Physical Metallurgy and Materials Science, 2016, 47, 5715-5721.	2.2	0
247	Advances and challenges in cryo ptychography at the Advanced Photon Source. AIP Conference Proceedings, 2016, 1696, .	0.4	0
248	Correlative 3D X-ray Fluorescence and Ptychographic Tomography of Frozen-Hydrated Green Algae. Microscopy and Microanalysis, 2019, 25, 114-115.	0.4	0
249	Uptake mechanisms of EGFR-targeted TiO2 nanoparticles Journal of Clinical Oncology, 2010, 28, e13583-e13583.	1.6	0
250	Optimized illumination for high-throughput ptychography. , 2019, , .		0
251	High-speed Three-dimensional Imaging at the Nanoscale via Fly-scan Ptycho-tomography. Microscopy and Microanalysis, 2020, 26, 1006-1008.	0.4	0
252	Three-dimensional reconstruction of integrated circuits by single-angle X-ray ptychography with machine learning. , 2021, , .		0

#	Article	IF	CITATIONS
253	Method development of X-ray ptychography: Towards high-resolution and high-throughput coherent imaging. , 2021, , .		0